The Bearingless 2-Level Motor

P. Karutz*, T. Nussbaumer**, W. Gruber*** and J.W. Kolar*
* ETH Zurich, Power Electronic Systems Laboratory, 8092 Zurich, Switzerland, karutz@lem.ee.ethz.ch
** Levitronix GmbH, Technoparkstrasse 1, 8005 Zurich, Switzerland
*** Johannes Kepler University Linz, Altenbergerstr. 69, 4040 Linz, Austria

Abstract– Several processes in chemical, pharmaceutical, biotechnology and semiconductor industry require contactless levitation and rotation through a hermetically closed chamber wall. This paper presents a novel concept that combines crucial advantages such as high acceleration capability, large air gap and a compact motor setup. The basic idea is to separate a homopolar bearing unit axially from a multipolar drive unit on two different height levels. Hence, the proposed concept is denominated as "Bearingless 2-Level Motor". In this paper, the bearing and drive functionalities are explained in detail and design guidelines are given based on analytic equations and electromagnetic 3D simulations. Furthermore, the influence of non-idealities such as saturation and coupling effects are evaluated and included in the design. Finally, measurements on an experimental prototype exemplify the design considerations and prove the excellent performance of the new concept.

I. Introduction

In the past decades there have been a lot of research activities in the field of bearingless motor drives [1] - [3]. The implementation of bearingless motor technology includes key features such as contactless operation, online tuneable bearing parameters, almost unlimited life time, wearless and lubrication-free operation and therefore a high level of purity. In the pharmaceutical, chemical, biochemical and semiconductor industry several processes require the application of chemical substances on rotating objects under clean room conditions [4]. Here, bearingless motors are of high interest for these applications. The advantage of the bearingless motor technology in these sensitive processes is its ability to spin a rotor in an encapsulated chamber, where the demand for high purity is satisfied and locally limited clean room space can be provided while avoiding failure susceptible seals.

Fig. 1 demonstrates schematically such a process, showing a levitated rotor carrying a process object. The process is enclosed by a chamber and the rotor is levitated and accelerated through the process chamber walls by the aid of electromagnetic bearings and drives, respectively. Basically, there are several requirements for these applications:

- A big air gap is required in order to ensure a minimum thickness and therefore mechanical robustness of the process chamber that is placed within the air gap.
- A compact motor setup is desirable due to the constantly increasing costs of clean room space.
- A high acceleration capability is needed in order to minimize the times between the process rotation speeds. This is directly influencing the efficiency and therefore the operating costs of the equipment.
- A maximum rotation speed required by the process has to be reached.
- A high temperature resistance is needed, including thermal expansion issues.
- A highly chemical resistant hardware setup avoids that the various strongly reactive chemicals degenerate the motor components.

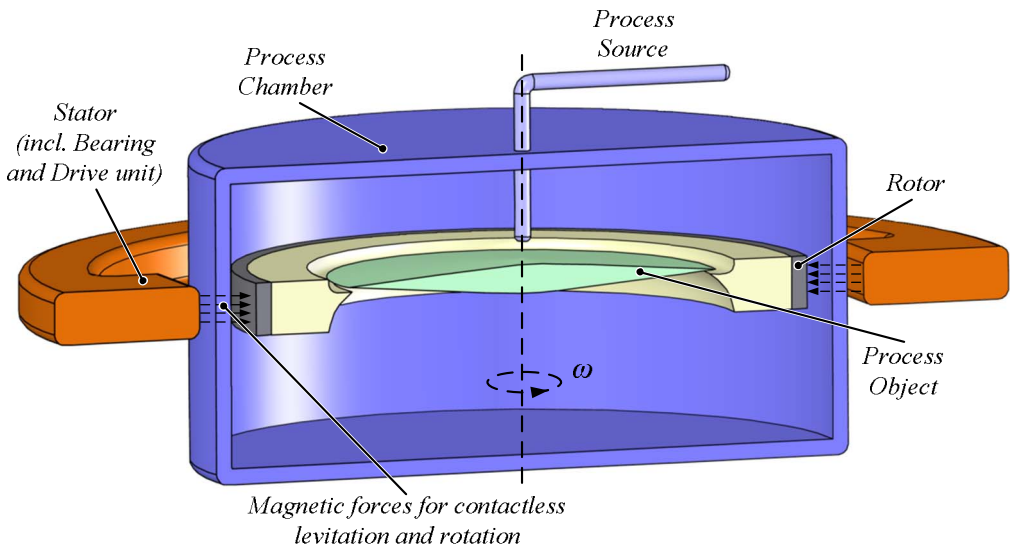

Fig. 1: Schematic cut view of an industry spinning process that is hermetically sealed within a process chamber, using magnetic bearing technology for the levitation of the rotor.

- A stable, vibration-free levitation and rotation has to be ensured within the whole operating range, i.e. potential axial, radial and tilting resonances must not effectuate significant axial and radial displacements of the rotor.

Obviously, not all requirements can be fulfilled simultaneously, since they are partially conflicting. However, in the past several concepts have been developed that showed good performance in one or more of the beforementioned aspects.

In [5], a setup for a magnetically levitated pump system for use in semiconductor, chemical and pharmaceutical industry has been introduced. It incorporates a combined iron path for the drive and the bearing windings. Here, a high number of stator claws levitates and drives a single permanent magnet impeller, where its radial position is controlled actively and the axial position as well as the tilting around the radial axes is controlled passively. Due to the nature of the concept a very high number of stator claws would be necessary to levitate rotors with large diameters (i.e. number of pole pairs). Therefore, this concept has been adapted in pump applications with a pole pair number of one and impeller diameters smaller than 100 mm.

Another concept has been presented in [6]. The concept features the utilization of the permanent magnet field of the rotor on different height levels for the drive and the bearing. The rotor can be built in a very compact way; however, due to the operation principle this concept uses only the stray flux components for the driving of the rotor, which results in a relatively low motor torque and a poor acceleration performance.

The bearingless segment motor with a combined bearing and drive has been presented in [7] and shows very good acceleration behaviour in combination with a compact setup. However, due to the coupled windings for bearing and drive the control of the motor gets very complicated. Furthermore, the cogging torque is quite critical for the segment motor. Additionally, the concept demands for a higher number of sensors and for increased power electronics effort.

In this paper, a new "Bearingless 2-Level Motor" is proposed, combining the advantages of the beforementioned concepts. In the following, the concept will be referenced as B2M. The principle of the B2M is explained in more detail in section II. In section III, the functionality of the magnetic bearing is introduced and analytical descriptions of stability are given. This is followed by a design procedure of the permanent magnet synchronous drive presented in section IV. Finally, the outstanding performance of the B2M is proven by measurements on a laboratory prototype in section V.

II. Principle of the 2-Level Motor Concept

The B2M concept introduced in this paper is based on the principle that the bearing and drive forces are applied on two different height levels (cf. Fig. 2). This enables a drive structure with significantly increased torque as compared to the concept presented in [6]. In comparison to the motors with integrated drive/ bearing functionality [7] the proposed 2-level concept shows a greatly reduced control effort and the advantage of separately optimised drive and bearing system.

A schematic cut view is depicted in Fig. 2. At the upper level, the magnetic bearing is located, consisting of rotor and stator permanent magnets (in order to provide a magnetic biasing) and the bearing windings around the four stator claws. The permanent magnet synchronous motor drive is positioned at an axially lower level. The rotor magnets are round-shaped and diametrically magnetized with alternately reversed polarisation direction. Additionally, the drive claws and windings are located between the bearing claws on the stator, wherefore a more compact setup can be achieved. Position and angular sensors are distributed around the stator for the detection of the radial position and the rotation speed.

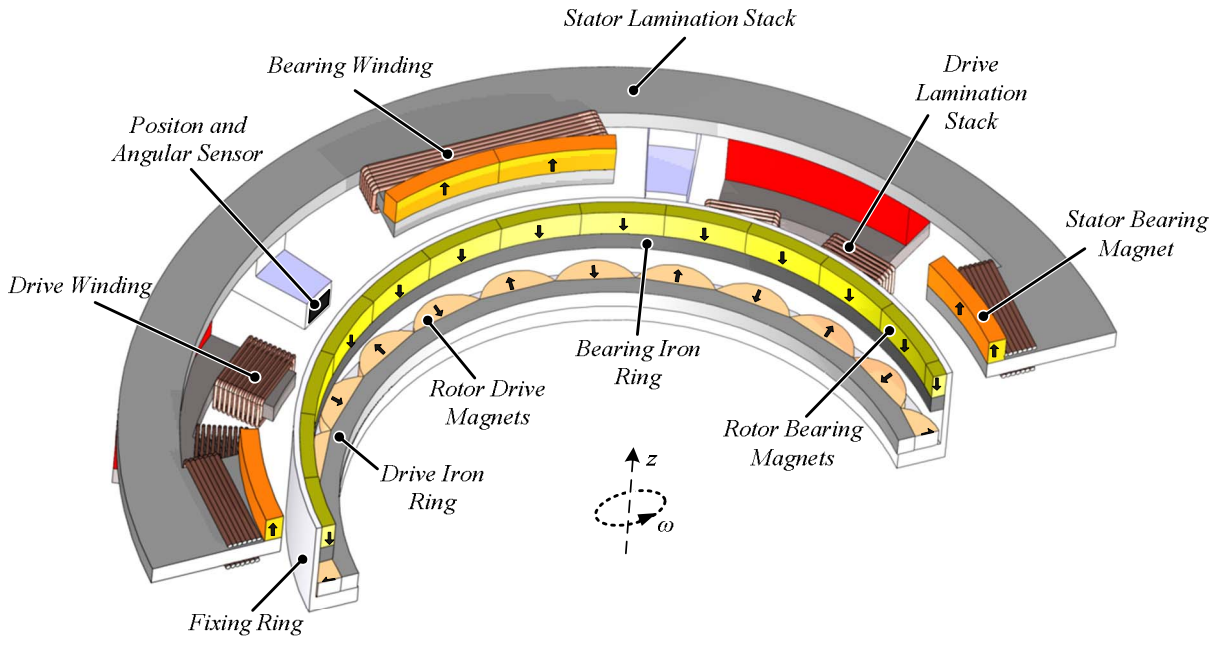

Fig. 2: Schematic cut view of the Bearingless 2-Level Motor including bearing and drive units on stator and rotor side.

III. Homopolar Magnetic Bearing

A. Design

In Fig. 3 the main components of the active radial bearing are depicted. The axial position and the tilting of the rotor is passively stabilized through reluctance forces in the air gap. The axial stiffness $k_{Z,B}$ [N/mm] describes the force [N] that is needed in order to move the rotor 1 mm out of its

stable position. The positive axial stabilization causes a negative destabilization in radial direction [8]-[10]. Hereby, the radial stiffness $k_{R,B}$ [N/mm] specifies the required force [N] needed to return the rotor back to its stable position after being displaced by 1 mm. Permanent magnets on both the stator and the rotor bearing iron ring are used for flux biasing and to define the flux path through the air gap. The flux density can be altered depending on the rotor position by supplying the bearing windings, thereby generating Maxwell-forces towards the target position [11]. The force-current factor $k_{I,B}$ [N/(A·turns)] describes the force that can be generated per ampere-turn of the bearing winding.

Generally, a high axial stiffness $k_{Z,B}$ is desired in order to counteract the weight force

$$k_{Z,B} \cdot \Delta z = m \cdot g \tag{1}$$

resulting in a minimum axial stiffness

$$k_{Z,B} > \frac{m \cdot g}{\Delta z_{\max}}, \tag{2}$$

where Δz_{max} is the maximum allowable displacement in the axial direction, m is the mass of the rotor and g is the gravitational constant.

However, as mentioned before, a high axial stiffness comes along with a destabilizing radial stiffness that has to be overcome by the stabilizing active magnetic force imposed by the bearing currents. Therefore, for allowing a maximum radial deflection Δr_{max} from the stable position, the force-current factor $k_{I,B}$ has to be larger than a minimum value given by

$$k_{I,B} > \frac{k_{R,B} \cdot \Delta r_{\max}}{N_B \cdot I_B}, \tag{3}$$

where N_B is the bearing coil winding number and I_B the bearing controller current. Here, it has to be considered

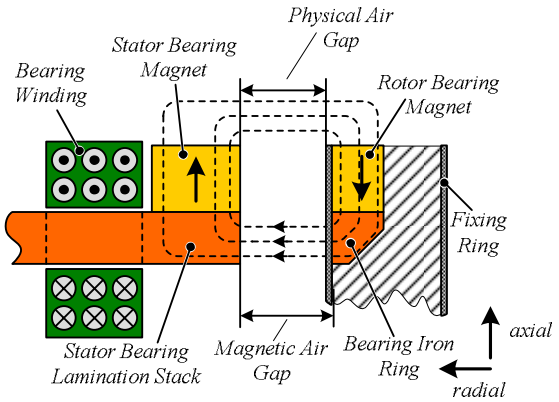

Fig. 3: Bearing principle of the Bearingless 2-Level Motor.

that the force-displacement dependency is non-linear; therefore, evaluating (3) with a linear radial stiffness $k_{R,B}$ is only valid within a limited operating range.

In order to facilitate the fulfilment of (3), N_B has to be chosen as high as possible. However, a high number of bearing turns decreases the current rise capability in the bearing inductance L_B. The electrical time constant of the bearing is given by

$$\tau_E = \frac{L_B}{R_B}, \tag{4}$$

where R_B is the winding resistance. Since L_B scales with N_B^2 and R_B with N_B, the electrical time constant increases linearly with N_B. For achieving a stable system control the condition

$$\tau_E << \tau_M, \tag{5}$$

with

$$\tau_M = \sqrt{\frac{m}{k_{R,B}}} \tag{6}$$

has to be satisfied, i.e. a small number of bearing windings is desirable from this point of view. Therefore the selection of N_B will always be a trade-off between high dynamics (cf. Eqs. (4) and (5)) and the maximum force condition (cf. Eq. (3)).

B. Interference with the drive system

Due to the axial and circumferential separation of the drive and bearing system the mutual coupling effects can be assumed to be low, wherefore general design considerations can be carried out separately. However, interactions between the bearing and the drive unit can cause tilting problems, which have to be considered and are addressed here now shortly.

In addition to the bearing's radial stiffness $k_{R,B}$, the diametrically magnetized permanent magnets of the drive on the rotor cause a magnetic force towards the stator leading to an additional destabilizing radial stiffness $k_{R,D}$ that has to be considered additionally in the bearing design. Besides the linear deflection along the axial or radial axis the tilting tendency of the bearing has to be investigated. Hereby, the destabilizing radial force of the drive $F_{R,D}$ causes a torque $M_{R,D}$ around the mass balance point with the height h of the rotor being the lever. At the same time the rotor is stabilized through the stabilizing bearing axial force $F_{Z,B}$ (provided by two of the four bearing windings) acting with a lever with the length of the effective radius r, causing a torque $M_{Z,B}$. The tilting tendency k_{Tilt} can therefore be described as the ratio of the two torques by

$$k_{Tilt} = \frac{M_{R,D}}{M_{Z,B}} = \frac{F_{R,D} \cdot h}{2 \cdot F_{Z,B} \cdot r} = \frac{k_{R,D} \cdot h^2 \alpha}{2 \cdot \frac{k_{Z,B}}{4} \cdot r^2 \alpha} = \frac{2 \cdot k_{R,D} \cdot h^2}{k_{Z,B} \cdot r^2}. \tag{7}$$

In order to guarantee a stable operation the condition $k_{Tilt} << 1$ has to be ensured.

An additional destabilizing torque on the drive level may be caused by the superimposed electromagnetic forces resulting from the drive winding currents. However, as will be shown in following section, for the pre-

sented B2M drive the opening angle of the drive lamination stack φ_D is selected equal to the angle of 180° electrical. With this, there will always be the same amount of attracting and repellent radial forces caused by the drive ampere-turns for any rotor position. Therefore, no resulting radial force acting on the rotor is caused by the drive current, which is why it is not considered in (7).

IV. Permanent Magnet Synchronous Drive

A. Basics

The main components of the permanent magnet synchronous drive [13] are depicted schematically in Fig. 4. The flux path is defined by the stator pole shoes with the two contrarily wound and series connected drive windings, the air gap and the round-shaped and alternating, diametrically magnetized magnets located on the rotor drive magnet ring. A motor torque M_D is generated if the drive windings are supplied with a rotation speed synchronized sinusoidal current, resulting in a tangential force F_T. Since permanent magnets always attract iron independently of their magnetization direction, the drive has priority positions defined by the constructive design (φ_D, w_{Claw}, d_{Claw}) the stator drive claw with respect to the rotor magnet dimensions and strength as

well as the size of the air gap. This behaviour causes a cogging torque $M_{Cogging}$, which can lead to jerky rotation especially in the low rotational speed range and has to be prevented by an optimisation of the stator claw design (see section IV.B).

The main drive parameters introduced depend mainly on the flux density distribution in the air gap. Since this distribution is highly non-linear and it is inexpedient to describe them analytically the subsequent design considerations are carried out using the 3D finite element simulation tool Maxwell® 3D [12].

B. Design

The mayor degrees of freedom for the permanent magnet synchronous drive design are the shape of the stator claws, especially the drive stator claw width w_{Claw}, the number of turns N_D of the drive coils and the thickness d_{IR} of the drive iron ring. By optimising these parameters the design aim of minimum cogging torque $M_{Cogging}$, acceptable radial stiffness $k_{R,D}$ and maximum motor torque M_D can be reached.

A first great reduction of the cogging torque can be achieved if the drive phases are circularly shifted by 90° electrically in order to avoid having two maximum field densities forcing the rotor into a preferred position. A further optimisation has to be carried out by simulations.

For simplifying the design simple U-shaped drive elements as depicted in Fig. 4 are considered here. As a detailed analysis shows, this shape does not lead to minimum cogging torque, however, to an optimal utilization of the available space for the drive. Since the cogging torque does not reach critical values due to the before-mentioned 90°-shifting of the phases, this shape is considered here. Furthermore, the opening angle φ_D is set to φ_D = 180° el.. This maximizes the achievable torque and leaves w_{Claw} as the only dimensional optimization parameter.

Fig. 5 shows the simulation results of $M_{Cogging}$, M_D and $k_{R,D}$ for different stator claw widths w_{Claw}. As can be seen there, a minimum cogging torque is reached for w_{Claw} = 20 mm at a high motor torque. Furthermore, Fig. 5 shows the linear dependency of the negative radial stiffness on the stator claw widths, which justifies the selection of w_{Claw} = 20 mm rather than any wider stator claw.

Another design parameter is the thickness d_{IR} of the drive iron ring, which constitutes the feedback path for the drive flux Φ_D. If d_{IR} is selected very small, saturation effects in the drive iron ring will occur and will degrade the flux density in the air gap and consequently the induced voltage and the drive torque. The critical thickness for d_{IR} is given at the connection point between two rotor magnets, since the maximum drive flux has to pass through there (cf. Fig. 4). The resulting flux density defining the saturation in the iron ring is composed of two flux components, where the major component is the permanent flux density by the drive permanent magnets and the minor component is the flux imposed by the drive winding currents. The distance between two stator

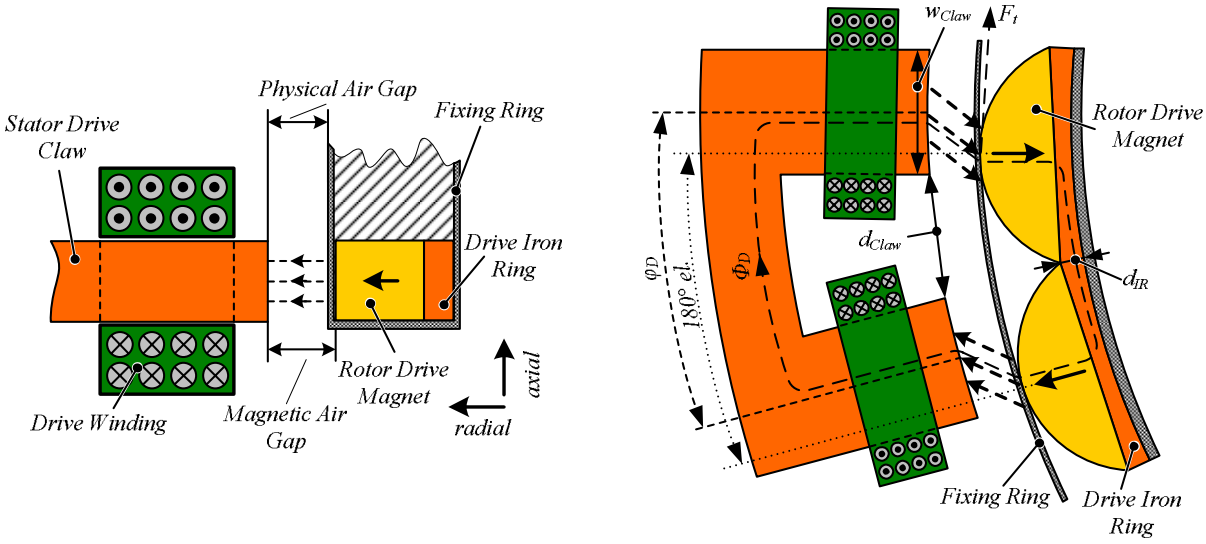

Fig. 4: Principle of the drive of the Bearingless 2-Level Motor with side view (left) and top view (right).

claws d_{Claw} is much smaller than the magnetic air gap δ_{mag} plus the length of the permanent magnets l_{PM} that add on to the flux path due to there air like permeability ($\mu_{mag} \approx 1$, cf. Fig. 6). Therefore, the current generated flux will mainly pass the through the space between the stator claws and hardly enter the rotor iron ring. Hence, the flux density in the iron ring will be clearly dominated by the permanent magnets. Thus, only this portion will be considered for the following design guidelines.

An integration of the approximately sinusoidal flux density distribution along the back side of half a drive magnet (cf. Fig.6) gives the total flux that passes from one magnet to the neighboured one through the iron ring

$$\Phi_D = \int B \cdot dA_{PM} = \int_0^{r\pi/2p} B_{PM} \cdot \sin\left(\frac{bp}{r}\right) \cdot h \cdot db = \frac{B_{PM} \cdot r \cdot h_{IR}}{p}, \quad (8)$$

In order not to saturate the iron material ($B < B_{Sat,Fe}$) at the position $\alpha = 0°$ the cross-section A_Φ has to fulfil the condition

$$A_\Phi \geq \frac{\Phi}{B_{Sat,Fe}}, \quad (9)$$

which gives with $A_\Phi = h_{IR} \cdot d_{IR}$ (cf. Fig. 6) the minimum thickness for the drive iron ring

$$d_{IR,\min} = \frac{B_{PM} \cdot r}{B_{Sat} \cdot p}. \quad (10)$$

The exact value of the flux density B_{PM} can be ascertained only by electromagnetic simulations. However, analytical approximations can already give a rough guideline. The maximum value of B_{PM}, which represents the worst-case condition for the saturation in the iron, occurs, when the air gap between rotor and stator becomes minimal, i.e. when the rotor magnets lie exactly in front of the drive claws as shown in Fig. 6. In this position, the flux density can be estimated (with $\mu_R \to \infty$) by

$$B_{PM,\max} \approx B_R \cdot \frac{l_{PM}}{l_{PM} + \delta_{mag}}, \quad (11)$$

where B_R is the remanence flux density of the permanent magnet, l_{PM} is the length of a permanent magnet, and δ_{mag} is the magnetic air gap (including the thickness of the sensor ring). Since in reality not all lines of the magnetic flux will follow the shortest way (and some not even enter the stator claw) and thus the average air gap will be larger than δ_{mag}, (11) represents a worst-case approximation. As a detailed analysis shows, at that considered maximum point the impressed force by the drive windings is zero, therefore the before-mentioned negligence of that influence has been correct.

Hence, (10) and (11) provide a guideline for the required iron thickness $d_{IR,min}$ in dependency of the pole pair number p and the radius r. However, selecting d_{IR} smaller than $d_{IR,min}$ relates to a weight reduction and can probably lead to an increased acceleration performance of the motor even though the air gap flux density is reduced.

Besides the discussed constructional parameters the winding number of the drive coils greatly influences the

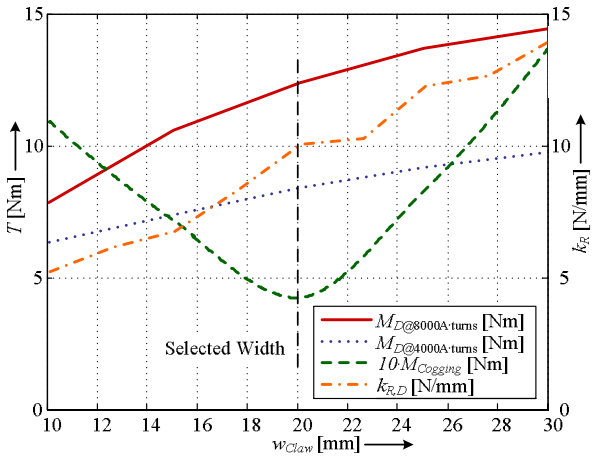

Fig. 5: Results of 3D finite element simulations for cogging torque $M_{Cogging}$, radial stiffness $k_{R,D}$ and motor drive torque M_D for two different ampere-turn ratios (per drive claw) in dependency on the stator claw width w_{Claw}.

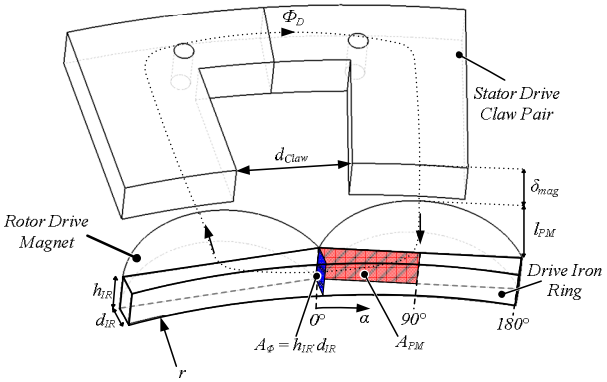

Fig. 6: Schematic view of a drive pole pair and the iron ring in front of a stator claw pair with flux cross section areas indicated.

acceleration behaviour of the B2M. The maximum applicable drive current is given by

$$I_D = \frac{-U_{ind} \cdot R_C \pm \sqrt{(R_C^2 + \omega^2 \cdot L_C^2)\, U_{DC}^2 - \omega^2 \cdot L_C^2 \cdot U_{ind}^2}}{R_C^2 + \omega^2 \cdot L_C^2}, \quad (12)$$

where U_{ind} is the rotation speed dependent induced voltage, R_C is the coil winding resistance, L_C the coil winding inductance, and $\omega = 2\pi \cdot n_R$ the electrical angular frequency.

As can be seen in Fig. 7 (a), for low rotational speeds the drive current is limited by the maximum current $I_{PE,max}$ provided by the power electronics, while for higher rotation speeds the current is decreasing due to the growing impedance $\omega \cdot L_C$ and due to the induced voltage which is increasing linearly with ω (cf. Fig. 7 (a)). Both $U_{ind} \sim N_D$ and $L_C \sim N_D^2$ are depending on the number of coil turns N_D, wherefore the available drive current is decreasing with increasing turns number (cf. Fig. 7 (a)). On the other hand, the drive power is given by the product of the induced voltage and the drive current

$$P_{Drive} = U_{ind}(N_D) \cdot I_{Drive}(N_D). \quad (13)$$

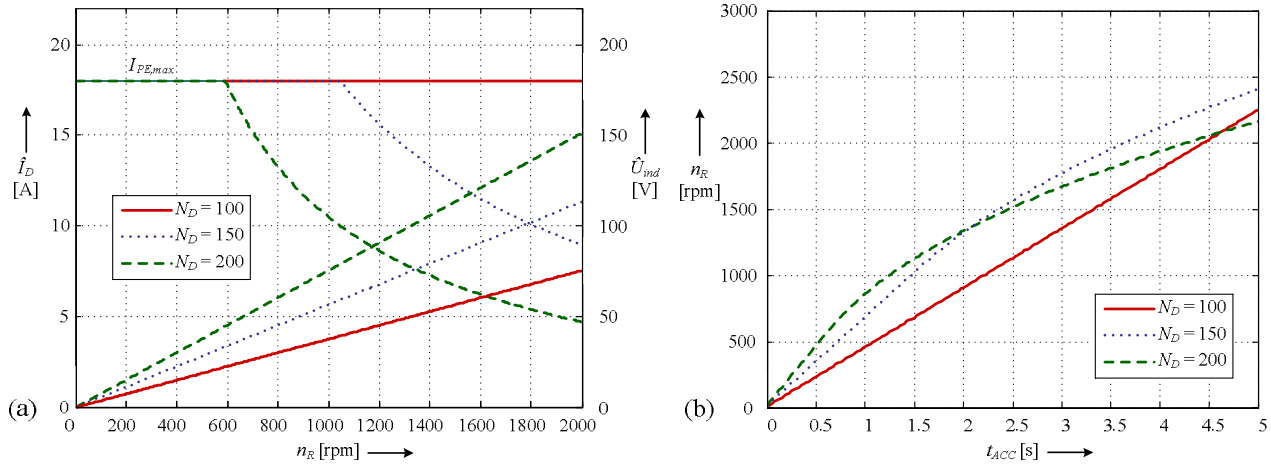

Fig. 7: (a) Achievable drive current $\hat{I}_D$ (for $I_{PE,\,max}$ = 18 A) and induced voltage $\hat{U}_{ind}$ in dependency of the rotation speed n_R for different coil winding numbers N_D and (b) estimated acceleration performance of the B2M.

Thus, an optimum number of turns can be identified for a certain rotation speed region. This is shown in Fig. 7 (b), where the acceleration times for different rotor speeds and winding numbers are plotted. It shows that a target rotational speed of 2000 rpm can be reached within 3.6 s for an optimum number of turns of N_D = 150. It has to be mentioned that this calculation is only correct for non-saturated material both in the stator claws and in the iron ring as discussed before.

V. Experimental Performance

Based on the design guidelines that have been presented in the previous sections, a prototype has been built in order to verify the design considerations. In Table 1 the characteristic parameters of the chosen design are compiled. Fig. 8 shows the complete assembly including the rotor and the stator-sided bearing and drive system. In Fig. 9 a better insight is provided into the constructional details of the setup. One can see the shape of the stator lamination stack and the 24 round-shaped permanent magnets (p = 12) placed between the drive positioning ring and the iron ring. The measured values of the axial and radial stiffness and the force-current factor are compared in Fig. 10 (a)-(c) with the simulated values and show generally a good agreement. For the axial stiffness (cf. Fig. 10(a)) the assumption of a linear factor $k_{Z,B}$ is correct in a wide area and the measured axial stiffness shows only a slight general deviation from the value predicted by the simulations. In contrast, the radial stiffness (cf. Fig. 10(b)), shows in reality a stronger nonlinear behaviour and therefore a bigger deviation from the linearized value in of the simulations. For the force-current factor, a perfect agreement between measurement and simulations can be seen in Fig. 10(c).

Finally, Fig. 11 shows the acceleration performance of the B2M drive from 0 rpm to 2000 rpm for $\hat{I}_{PE,max}$ = 18 A. For the run-up sequence, the final speed of 2000 rpm can be reached within 3.8 s, which is close to the value predicted by the simulations (cf. section IV.B), while the deceleration is accomplished within 2.8 s. This performance is very satisfactory considering the motor dimensions and the large air gap. With this, on the one hand the design procedure and correctness of the simulations could be verified, and on the other hand the excellent performance of the B2M concept could be proved.

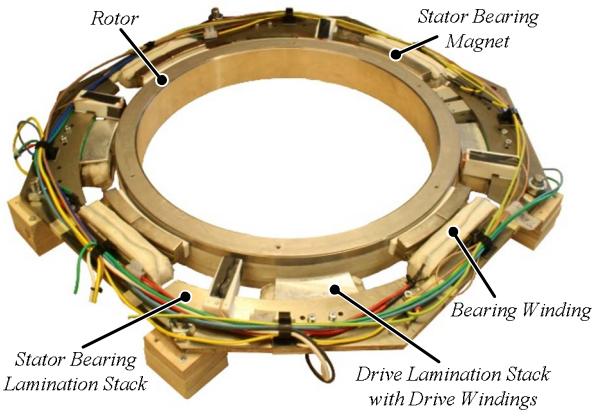

Fig. 8: Photography of completely assembled laboratory proto type with bearing and drive windings.

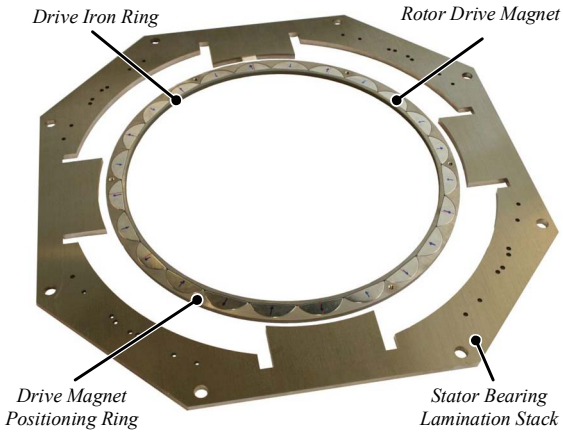

Fig. 9: Photography of rotor inside showing round-shaped drive magnets being placed between the drive iron ring and the drive magnet positioning ring.

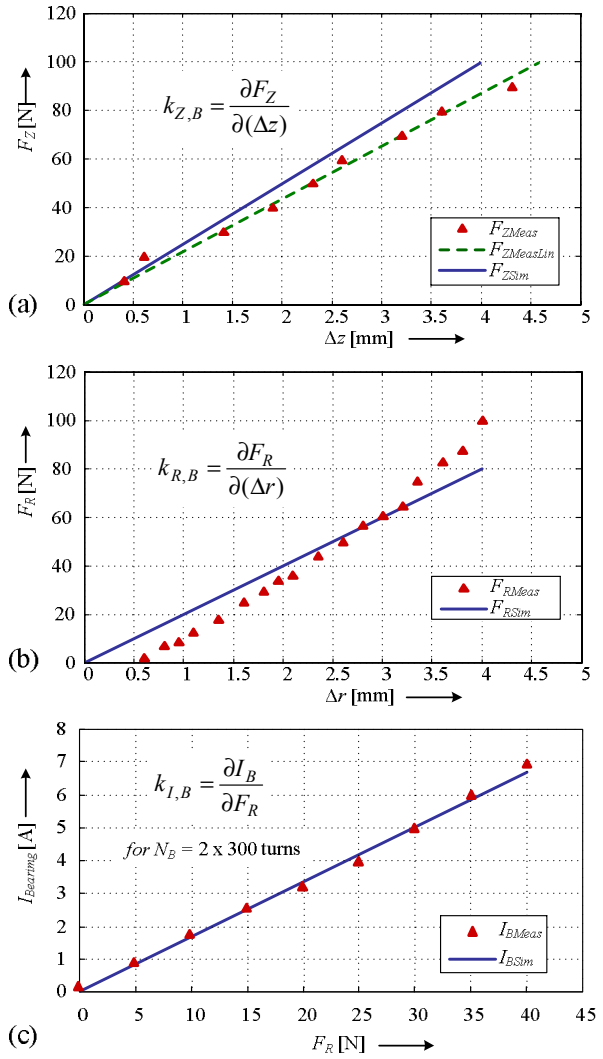

Fig. 10: (a) Measured and simulated axial stiffness; (b) measured and linearized simulated radial stiffness; and (c) measured and simulated force-current factor.

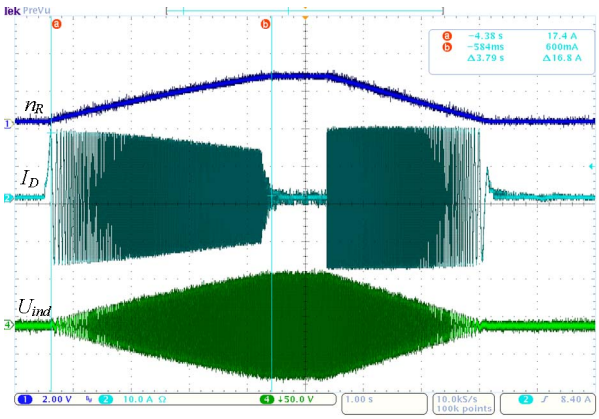

Fig. 11: Acceleration performance of B2M from 0 to 2000 rpm for $I_{PE,max}$ = 18A in 3.8s and deceleration in 2.8s (scales: 1600 rpm/div., 10 A/div., 50 V/div., 1 s/div.). For the measurement of the induced voltage a separate measurement coil with the winding number of a half phase (2 x 150 turns) has been used.

TABLE 1: DESIGN DATA OF THE EXPERIMENTAL SETUP

Outside rotor diameter	410 mm
Mechanical air gap δ_{Mech}	7 mm
Number of pole pairs p	12
Axial stiffness $k_{Z,B}$	25 N/mm
Radial stiffness $k_{R,B}$	-20 N/mm
Force-Current factor $k_{I,B}$	1 N/(100 A·turns)
Tilting stiffness $k_{\varphi,B}$	1 N/°
Motor Moment M_D for I_D = 1A	0.7 Nm
Cogging Torque $M_{Cogging}$	0.45 Nm
Bearing phase winding number N_B	2 x 300 turns
Drive phase winding number N_D	4 x 150 turns
Rotor mass m	5 kg

VI. CONCLUSIONS

The paper describes a new concept called "Bearingless 2-Level Motor" (B2M) that is of high interest for several industry branches, where contactless levitation and rotation in clean room environments is required. The new concept features high acceleration capability, a compact setup, low power electronics effort and a separate design and simple control of the bearing and drive units even for large air gaps. In this paper, the functionality of the B2M concept has been explained and guidelines for the design of the drive and bearing unit have been presented, also taking saturation and coupling effects between the drive and bearing system into account. Finally, the theoretical considerations have been verified on a prototype setup by measurements of design parameters and achievable acceleration times.

REFERENCES

[1] R. Schoeb, N. Barletta, "Principle and Application of a Bearingless Slice Motor," *JSME Int. Journal Series C*, pp. 593-598, 1997.

[2] A. Chiba, D.T. Power, M.A Rahman, "Chracteristics of a Bearingless Induction Motor," *IEEE Trans. Magnetics*, vol. 27, no. 6, Nov. 1991.

[3] S. Silber, W. Amrhein, P. Boesch, R. Schoeb, N. Barletta, "Design aspects of bearingless slice motors," *IEEE/ASME Trans. Mechatronics,* vol. 10, no.6, pp. 611-617, Dec.2005.

[4] Y. Chisti, M. Moo-Young, "Clean-in-place systems for industrial bioreactors: Design, validation and operation", *Journal of Industrial Microbiology and Biotechnology*, 1994.

[5] N. Barletta, R. Schöb, "Design of a Bearingless Blood Pump," *3rd Int. Symp. on Magnetic Supspension Technology*, Tallahassee, 1995.

[6] T. Schneeberger, J. W. Kolar, "Novel Integrated Bearingless Hollow-Shaft Drive," *Proc. of the IEEE Ind. Applic. Conf. IAS*, Tampa (USA), 8 – 12 October 2006.

[7] W. Gruber, W. Amrhein, "Design of a Bearingless Segment Motor," *Proc. of the 10th Int. Symp. on Magnetic Bearings* Martigny, 2006.

[8] J. Delamare, E. Rulliere, J.P. Yonnet, "Classification and synthesis of permanent magnet bearing configurations," *IEEE Trans. Magnetics*, vol.31, no.6, pp 4190-4192, Nov. 1995.

[9] J.-P. Yonnet, "Permanent magnet bearings and couplings", *IEEE Trans. Magnetics*, vol.17, no.1, pp. 1169- 1173, Jan. 1981.

[10] S. Earnshaw, "On the nature of the molecular forces which regulate the constitution of the luminiferous ether," *Trans. Camb. Phil. SOC.*, vol. 7, no. 1, pp. 97-112, 1839.

[11] W. Amrhein, S. Silber, K. Nenninger, "Levitation forces in bearingless permanent magnet motors", *IEEE Trans. Magnetics*, vol.35, no. 5, pp. 4052-4054, Sep. 1999.

[12] Maxwell® 3D by Ansoft Corporation, http://www.ansoft.com.

[13] D.P.M. Cahill, B. Adkins, "The permanent magnet synchronous motor," *Proc. Inst. Elec. Eng.*, vol. 109, no. 48, pp. 483-491, Dec. 1962.